Structure of a Triglyceride Microemulsion: A Small-Angle Neutron Scattering Study

S. F. Trevino*

Polymer Research Branch, U.S. Army Research Laboratory, APG Maryland 21005-5069, and Center for Neutron Research, National Institute of Standards and Technology, Gaithersburg, Maryland 20899

R. Joubran and N. Parris

U.S. Department of Agriculture, Eastern Regional Research Center Agricultural Regional Service, Philadelphia, Pennsylvania 19118

N. F. Berk

Center for Neutron Research, National Institute of Standards and Technology, Gaithersburg, Maryland 20899

Received: April 30, 1997; In Final Form: September 30, 1997

The microscopic structure of a microemulsion of triolein oil, aqua (water−ethanol, 80/20 wt %), and polyoxyethylene (40) sorbitol hexaoleats has been studied with small-angle neutron scattering. Contrast variation (in the scattering of neutrons) is accomplished by the deuteration of the aqua and oil components of the system. Samples for which only the aqueous phase is deuterated reveal the geometry of the aqueous phase, and those in which only the oil is deuterated reveal the geometry of the oil phase. Finally, when both oil and aqua are contrast matched by deuteration, the surfactant geometry is measured. The aqueous−surfactant surface and the oil−surfactant surface are found to be of significantly different geometries. These two surfaces are described in detail for varying aqua concentration by the very successful leveled-wave model. The behavior of the leveled-wave model parameters produced by the aqua geometry, as a function of aqua concentration and temperature, correlates with a thermodynamic instability in the miscibility. Further, the spectrum of neutrons produced by the surfactant itself is different from the aqua and oil spectra. Although a detailed geometric description of the surfactant is not available for this component (no geometric model being applicable), the data are consistent with there being different geometries for the two bounding surfaces. A plausible correlation between the geometric behavior of the material and a miscibility gap is also detected.

Introduction

Microemulsions have been defined as stable dispersions of water, oil, and amphiphiles having diameters less than 1400 Å.[1] Most microemulsions are prepared from normal alkanes, but a few examples of triglyceride microemulsions have been reported in the literature.[2−5] Alendar and Warenheim[4,5] have compared the triglyceride behavior of microemulsions to that of ordinary hydrocarbons. They concluded that triglycerides, in particular long-chain fatty-acid glycosides such as those of peanut oil, were considerably more difficult to solubilize into microemulsions than hydrocarbons or alkyl esters. Gulik-Krzywicki and Larsson[6] studied the structure of the reversed micelle solution (L_2) in systems containing water, soybean oil, and monoglyceride using freeze-fracture electron microscopy. Electron micrographs of the L_2 phase indicated that small smooth lamellae were oriented into stacks. Fontell et al.[7] reported on the structural relationship of systems containing liquid-crystalline and isotropic liquid L_2 phases. They identified transitions between the two states as a result of changes in either temperature or composition of these systems. It can therefore be concluded that the structure of the reversed micelle aggregates in the L_2 solution closely resembles that of both the lamellar and the hexagonal liquid-crystalline phases.

Recently, a separated phase has been identified for a system containing polyoxyethylene (40) sorbitol hexaoleates, soybean oil, and an aqueous phase composed of water/ethanol (80/20 wt %).[8] The phase diagram is presented in Figure 1 for two temperatures. This figure reveals an instability in miscibility (producing a two-phase region) as a function of temperature at an aqua concentration near 25% by weight along the 40/60 line of oil−surfactant composition.[9] The phase diagram remains "connected" at temperatures above 22 °C. In a previous work,[10] we characterize the microscopic structure of the aqua−surfactant surface of this microemulsion by small-angle neutron scattering. To do this, we deuterated the aqueous component so as to

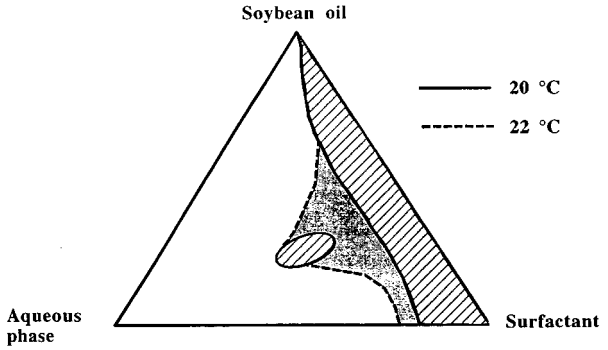

Figure 1. Phase diagram of the system with soybean oil, surfactant, and aqua components for two temperatures. Hatched regions correspond to stable microemulsion at 20 °C. These regions, in addition to shaded regions, correspond to stable microemulsion at 22 °C and higher temperatures.

S1089-5647(97)01459-4
Published on Web 01/16/1998

TABLE 1: Physical and Neutron Scattering Properties of the Substances Used in This Work

label	substance	density d (gm/cm^3)	molecular weight (amu)	stochiometry	scattering length $b = \Sigma_i n_i b_i^a$ (cm $\times 10^{-12}$)	molecular volume $V = W/A_d$ (cm^3 $\times 10^{-24}$)	scattering length density $\rho = b/V$ (cm^{-2} $\times 10^{12}$)
	H_2O	1.0	18.0	H_2, O	−0.1677	29.88	−0.005 61
	D_2O			D_2O	1.9153		0.064 10
E_h	ethanol	0.8	47.0	C2, H6, O	−0.3345	97.54	−0.003 43
E_d	ethanol-d_5			C_2, D_5, H, O	4.873		0.051 04
O_h	triolein-H_{104}	0.92	885.4	C57, H104, O6	2.4702	1597.86	0.001 55
O_d	triolein-D_{104}			C57, D104, O6	110.79		0.069 33
S	surfactant	1.01	3512.0	C194, H352, O52	27.474	5773.25	0.004 76
A_{d1}	aqua (0.816/0.184 wt) D_2O/E_h = (0.762/0.238 vol) D_2O/E_h						0.048 0
A_{d2}	aqua (0.8/0.2 wt) D_2O/E_d = (0.763/0.237 vol) D_2O/E_d						0.060 76
A_m	aqua−surfactant match						0.003 87

[a] Sum over i atoms of molecule, n_i number and b_i neutron scattering length of type i nucleus, respectively. The scattering lengths of the various isotopes used are C, $b = 0.6648 \times 10^{-12}$ cm; H, $b = -0.3741 \times 10^{-12}$ cm; D, $b = 0.6674 \times 10^{-12}$ cm; O, $b = 0.5805 \times 10^{-12}$ cm.

produce significant contrast for neutron scattering between the aqueous component and the remainder of the system. We found that for high aqueous concentrations (35−40 wt %), the results were consistent with a bicontinuous structure, and equally important we found that for low aqueous concentrations (<25 wt %) substantial spatial correlations exist for the aqueous component.

In this work we aim to complete the characterization of the geometry of all the components of the microemulsion approximately along the line of constant oil−surfactant (0.4/0.6) concentration. In so doing, we hope to discover a mechanism that correlates with the thermodynamic instability mentioned above. We wished to obtain measurements on samples in which the oil component is deuterated. For technical reasons it was not possible to obtain or synthesize deuterated soybean oil, which we used in our previous work.[10] Instead, in this work we use triolein oil, which differs from soybean oil in that on average there are four fewer unsaturated carbons. Despite the minor differences between soybean and triolein oils, we do not expect the geometric properties of the microemulsions produced with these two oils to differ qualitatively.

We are also aware that the phase diagram may be affected by deuteration of several of the components. It would however be extremely surprising if the qualitative nature of the behavior of the components was greatly affected by these changes. Several studies have been reported[11,12] whose aims were to discover the effect of deuteration upon the phase diagram and geometry of selected microemulsions. These studies revealed that although the phase diagram is changed (albeit not dramatically), the geometry of the various components remains unchanged. Even in the one case[12] in which bulk properties showed substantial deuteration effects, the structural effects were minimal. We therefore feel confident that data obtained from the deuterated samples will reflect a consistent geometry of the various components.

We present data here for samples in which (a) only the aqua phase is deuterated, revealing the shape of the aqua−surfactant surface; (b) the oil phase is deuterated, while the remainder remains protonated, revealing the oil−surfactant surface geometry; and (c) the oil and aqueous phases are deuterated and contrast matched, while the surfactant remains protonated, exposing the shape of the surfactant.

The necessary terminology and technological discussion concerning the neutron scattering method and the leveled wave model can be found elsewhere.[10] We recommend that work to the reader and,with the exception of a discussion of the role of the log-normal distribution in the leveled-wave model, provide little further exposition here. An excellent review article by Chen[13] is also recommended.

Experimental Section

Sample Preparation. The deuteration of the aqueous phase component is easily accomplished, since both deuterated water and ethanol are available commercially. We synthesized fully deuterated triolein oil (1,2,3-tris[*cis*-9-octadecenoyl]glycerol) by reacting deuterated oleic acid (purity, isotopic = 98%, chemical = 90%) with deuterated glycerol in toluene for 5 days at 108 °C. The triglyceride was purified with a 1-ft silica gel column and 85:15 v/v hexane/ethyl acetate as the eluent. Purified fractions used for the neutron scattering measurements contained 99% chemically pure deuterated triglycerides (verified by nuclear magnetic resonance). The preparation of the deuterated triolein was expensive and time-consuming. We had no means of preparing samples other than those presented here.

Table 1 presents the sample properties and calculated neutron scattering densities of the several components used throughout the present measurements.

Small-Angle Neutron Scattering. Two small-angle neutron scattering (SANS) instruments were used in the present study. The data for samples of deuterated aqua were obtained at the W. C. Koehler SANS facility of the Oak Ridge National Laboratory.[14] For these measurements, the samples were contained in quartz cells 2 mm thick. A wavelength of 4.75 Å was used throughout, and several sample to detector distances were used to obtain the Q range reported here. The remainder of the data were obtained at the Cold Neutron Research Facility (CNRF) of the National Institute for Standards and Technology (NIST).[15] A wavelength of 5 Å was used throughout, and again various sample to detector distances were used to obtain the Q range. The samples for the CNRF measurements were contained in cells similar to the Oak Ridge cells but of 1 mm thickness.

The temperature of the samples in all measurements was controlled by circulation of a temperature-controlled liquid through the sample holder block. Temperature control of 1/3 °C is easily attained with this device. The temperature of the samples was varied beginning with the highest temperature and decreasing, under computer control, to the lowest. The samples were examined visually at the end of this procedure to determine that they were not turbid. Net counts for each sample are obtained in the usual way by subtraction of blank and beam-off counts and correction for detector efficiency. Azimuthal averages of the data from the two-dimensional detectors are then

TABLE 2: Results of the Leveled-Wave Fit to Aqua Structure Data[a]

sample	C_o	k_s (Å^{-1})	Q_p (Å^{-1})	Σ (Å^{-1})	I_o (cm^{-1})	I_{calc} (cm^{-1})	composition
A1 20 °C	0.145	0.0831	0.0650	0.0397	6.51	5.05	oil 34.1 wt %
A1 25 °C	0.145	0.0842	0.0650	0.0414	6.74	4.87	surf 51.2 wt %
A1 30 °C	0.145	0.0817	0.0645	0.0386	6.92	5.35	aqua 14.7 wt %
A2 20 °C	0.172	0.0786	0.0615	0.0370	9.15	6.88	oil 32.8 wt %
A2 25 °C	0.172	0.0768	0.0603	0.0365	9.83	7.38	surf 49.2 wt %
A2 30 °C	0.172	0.0769	0.0605	0.0369	10.4	7.33	aqua 17.5 wt %
A3 20 °C	0.217	0.0719	0.0553	0.0354	15.4	10.8	oil 30.8 wt %
A3 25 °C	0.217	0.0715	0.0560	0.0350	16.4	10.9	surf 46.3 wt %
A3 30 °C	0.217	0.0698	0.0563	0.0309	16.6	11.7	aqua 22.9 wt %
A4 20 °C	0.271	0.0671	0.0528	0.0306	23.0	15.4	oil 28.8 wt %
A4 25 °C	0.271	0.0644	0.0516	0.0277	24.3	17.4	surf 43.2 wt %
A4 30 °C	0.271	0.0618	0.0506	0.0260	26.3	19.6	aqua 28.1 wt %
A5 20 °C	0.316	0.0591	0.0491	0.0234	31.3	24.6	oil 27.0 wt %
A5 25 °C	0.316	0.0567	0.0476	0.0207	32.8	27.8	surf 40.6 wt %
A5 30 °C	0.316	0.0562	0.0466	0.0223	38.5	28.6	aqua 32.4 wt %
A6 20 °C	0.368	0.0511	0.0441	0.0174	48.0	41.0	oil 25.0 wt %
A6 25 °C	0.368	0.0516	0.0442	0.0176	51.8	39.9	surf 37.5 wt %
A6 30 °C	0.368	0.0487	0.0422	0.0155	54.9	47.4	aqua 37.5 wt %

[a] C_o is the volume fraction of the aqua component. Samples are made from component A_{d1} for aqua, O_h for oil, and S for surfactant from Table 1. I_o, k_s, and Σ are parameters of the leveled-wave model which fit data. Q_p is the value of Q at which the peak occurs in $I(Q)$, and $I_{calc} = 4\pi C_o(1 - C_o)(\Delta\rho)^2/k_s^3$ is the expected peak intensity.

calculated and absolute cross sections obtained (after correction for sample thickness and transmission) by comparison with well-characterized secondary standards. A description of the instrumentation is given elsewhere[14,15] along with an abbreviated exposition of the neutron scattering theory useful for the understanding of this technique.

Results and Discussion

The data presented here are in absolute units of the specific scattering cross section $d\sigma/d\Omega$, in units of cm^{-1}.

In this work we use the log-normal distribution[16] in the data analysis in several contexts, and it is useful here to establish the exact meaning of the notation for clarity. In Johnson's notation,[16] the probability density function for the log-normal distribution is given as

$$p(x) = [x\sigma\sqrt{2\pi}]^{-1} \exp[(-1/2)\{\ln(x) - \zeta\}^2/\sigma^2] \quad (1)$$

where ζ and σ^2 are the expected value and variance of the Gaussian distribution of $\ln(x)$. In terms of these parameters, the peak of the function is located at x_s, where

$$x_s = \exp(\zeta - \sigma^2) \quad (2)$$

so that one can rewrite $p(x)$ as

$$p(x) = [x\sigma\sqrt{2\pi}]^{-1} \exp[(-1/2)\{\ln(x/x_s) + \sigma^2\}^2/\sigma^2] \quad (3)$$

In the various fitting procedures described below, the parameters x_s and σ are considered the independent variables. However, from a physical view, it is more appropriate to describe the features of $p(x)$ by the variables x_s and Σ^2, where Σ^2 is the variance of $p(x)$ about x_s. This latter variable is given by

$$\Sigma^2 = \int (x - x_s)^2 p(x)\, dx \quad (4)$$

$$\Sigma^2 = x_s^2[\exp(4\sigma^2) - 2\exp(3/2\sigma^2) + 1] \quad (5)$$

In the leveled-wave model, the geometry of the surface separating the contrasted components is constructed by "... leveled sets—two-dimensional contours—of a stochastic standing wave $S(\mathbf{r})$, which is defined by"[17]

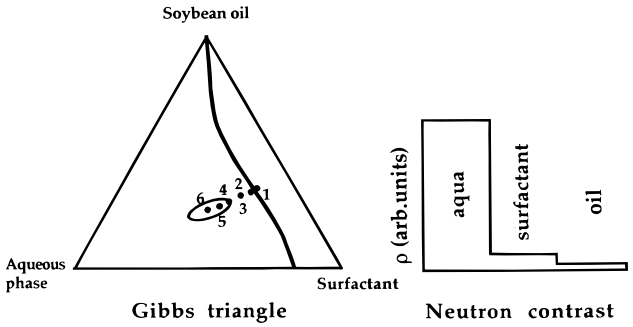

Figure 2. Composition of six samples used for measurement of the aqua structure. Solid lines correspond to 20 °C phase boundaries (Figure 1) shown for reference. Bar graph indicates specific neutron contrast of three components used in samples.

$$S(\mathbf{r}) = (N\langle A^2\rangle)^{-1/2}\Sigma A_n \cos(\mathbf{k}_n\cdot\mathbf{r} + \phi_n) \quad (6)$$

in which the direction of the N wave vector $\mathbf{k}_n$, amplitudes A_n, and phases ϕ_n are chosen randomly. In the present work, the distribution $p(k)$ of the magnitude of $\mathbf{k}_n$ is chosen to be the log-normal of eq 1. Thus the parameters that define the geometry of the interface, from which the neutron scattering properties are calculated, are k_s and σ of this distribution. As stated above, we report k_s and Σ obtained from a fit to the data. The leveled-wave model is designed to describe the more or less static geometry of an interface having a well-defined length scale and to obtain the scattering function $I(Q)$ which such a geometry would produce. As such, it does not describe, for example, the thermal fluctuations of a liquid which produce an increase in $I(Q)$ at small Q or other mechanisms which might produce such an effect. In the analysis of our data we will rely solely on the leveled-wave model, where applicable, since it captures the geometry that concerns us here.

Aqua Structure. The aqua structure is determined from samples in which we use D_2O to make the neutron contrast for the aqua component substantially different from that of the remaining material. Table 2 contains the labels and composition of the six samples, and Figure 2 presents a schematic representation of their position on the Gibbs triangle and the contrast achieved for this purpose (based on the data from Table 1). It is clear that although the oil and surfactant are not perfectly matched, they are, with respect to the aqua, essentially the same.

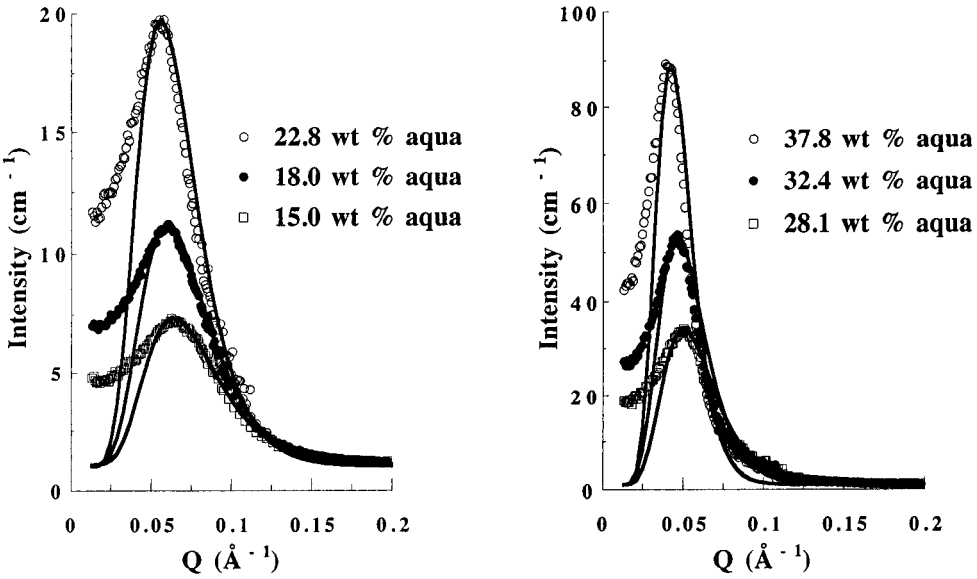

Figure 3. SANS data obtained from six samples used for the aqua structure determination at 30 °C. Solid lines are a fit of data with the leveled-wave model. Different scales are used for clarity.

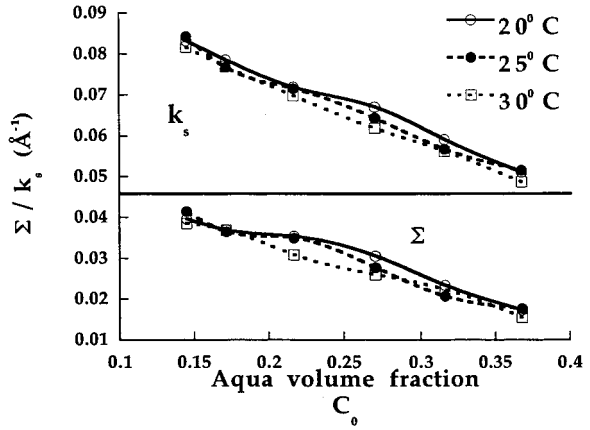

Figure 4. Parameters k_s and Σ plotted for three temperatures (present measurements). C_o is the volume fraction of the aqua component; k_s and Σ^2 are the k scale and variance of the log-normal distribution of wave vectors used to describe the aqua structure in the leveled-wave model (see text). One standard deviation in the value of these parameters is smaller than the symbols.

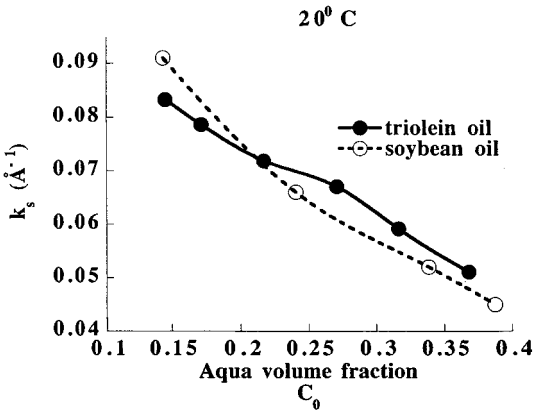

Figure 5. Comparison of aqua structure for microemulsions with triolein oil (present work) and with soybean oil (ref 10). C_o is the volume fraction of the aqua component.

These data reveal the aqua−aqua spatial correlations, that is, the geometry of the aqua−surfactant surface.

SANS spectra were obtained for the six samples at temperatures of 20, 25, and 30 °C. Figure 3 presents the data obtained at 30 °C for all six samples. The data are presented on two ordinate scales for clarity. The solid lines result from a fit to the data with the leveled-wave model.[10,17] The resulting parameters are given in Table 2. Although not perfect, especially at small Q where thermal fluctuations and finite compressibility of the liquid may be important (and are ignored by the leveled-wave model), the fits are adequate for a description of the data and therefore of the time-averaged geometry of the aqua−surfactant surface. (The data resulting for the two other temperatures are very similar to the above and are not presented. They have, however, also been fit with the leveled-wave model.) Table 2 also gives the position Q_p of the peak in the intensity $I(Q)$, which is not the same as k_s.[17] The two parameters, k_s and Σ, which thus determine the geometry of the aqua−surfactant surface are plotted in Figure 4 as functions of C_o, the volume fraction of the aqua component (the standard deviation of these parameters is smaller than the symbols). Both parameters are monotonic functions of C_o for 30 °C but show significant departures from this behavior for the lower temperatures; these departures become most pronounced at 20 °C. They occur near a concentration of 25% aqua, which is near the thermodynamic instability of miscibility. It seems reasonable to associate this behavior with this thermodynamic instability. We did not notice this behavior in the previous work on the soybean oil microemulsion.[10] The oversight was clearly a result of using too few values of the aqua concentration in that study, as shown in Figure 5. This figure displays the data for microemulsions using soybean oil[10] and using triolein oil (this work) for a temperature of 20 °C. Without the two data points for aqua volume fractions of ∼27 and 33% in the present work, the phenomenon could have easily been missed. This figure also reinforces our contention that the geometry of the microemulsion is not qualitatively different between that using soybean oil and that using triolein oil, at least of the aqua component.

Figure 6 shows the geometry that is described by the parameters of the leveled-wave model. This figure plots a slice of the three-dimensional distribution of the aqua as one component and the remainder as the other for the two extremes of aqua concentration used here. It is clear that for the highest aqua concentration the geometry is consistent with a bicontinuous structure. It is also clear that for the lowest concentration

TABLE 3: Oil Structure Leveled-Wave Model and Guinier Fit

			leveled-wave paramaters[a]			Guinier parameters[a]		composition			
oil samples	temp (°C)	I_o	k_s (Å^{-1})	Q_p (Å^{-1})	Σ (Å^{-1})	I_g	R_g (Å)	oil	surf	aqua	oil C_o
O11	22.5	15.56	0.0532	0.0281	0.0620	62.29	56.68	32.5	48.7	18.8	0.325
O12	25.0	18.35	0.0478	0.0294	0.0418	71.80	66.70	32.5	48.7	18.8	0.325
O21	16.5	19.57	0.0515	0.0285	0.0554	94.84	45.90	27.9	46.9	25.2	0.276
O22	19.7	27.91	0.0454	0.0246	0.0502	133.27	69.50	27.9	46.9	25.2	0.276
O23	20.0	27.11	0.0457	0.0266	0.0443	117.73	69.50	27.9	46.9	25.2	0.276
O31	11.0	28.71	0.0463	0.0284	0.0406	121.94	65.13	24.6	44.2	31.2	0.243
O32	13.0	28.98	0.0457	0.0272	0.0428	125.82	69.73	24.6	44.2	31.2	0.243
O33	15.0	27.49	0.0461	0.0277	0.0423	112.67	69.50	24.6	44.2	31.2	0.243

[a] See text for definition of parameters.

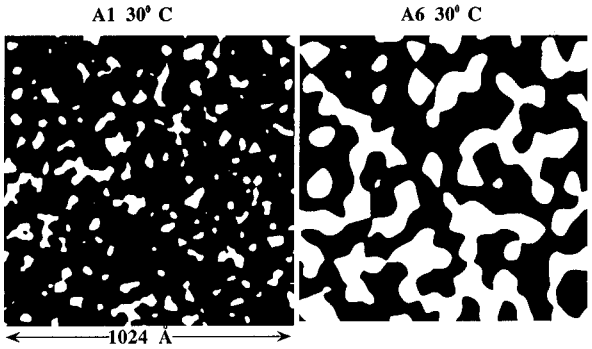

Figure 6. Geometry of aqua component obtained using the log-normal distribution of wave vectors obtained from the leveled-wave model and parameters derived from the data (Table 2). White regions correspond to the aqua component and dark regions to the other two. (Samples labeled as in Table 2.)

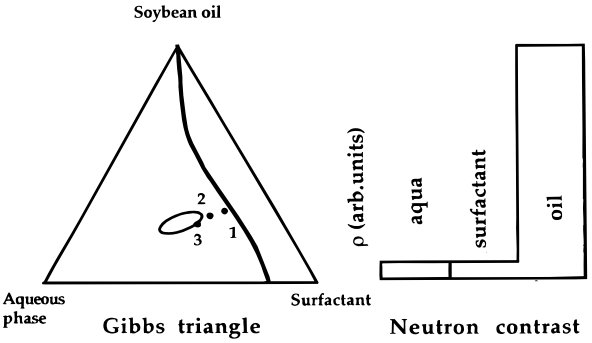

Figure 7. Neutron contrast and composition of three samples used for the measurement of oil structure. Solid lines correspond to the 20 °C phase boundaries (Figure 1) (shown for reference).

the aqua component does not consist of spherical droplets but rather of a still well-correlated structure that is describable by a rather narrow distribution of length scales.

Oil Structure. Three samples were prepared in which only the triolein oil is deuterated fully. There was very little deuterated oil left when these samples were made, most of it having been expended in the surfactant structure samples (see below). Table 3 shows the labels and concentrations of the components for these three samples. Figure 7 gives a schematic of the position of the three samples on the Gibbs triangle and the neutron scattering length densities of the various components. In these samples, the aqueous phase consists of a mixture of water ethanol in a ratio of 4/1, with the water made up of 82% H_2O and 18% D_2O (aqua sample A_m of Table 1). This concentration produces an aqueous phase with a neutron contrast that nearly matches that of the natural surfactant.

Figure 8 presents all the data obtained from the three samples. Included are the results of fits with two terms, the first representing the leveled-wave model for the peak in the data and the second a Guinier function to describe the smallest angle scattering, I_g being the prefactor and R_g the radius of gyration. We have included the Guinier function here because of the substantial overlap of this rapidly varying (with Q) component and the peak in the spectrum. We do not have sufficient data at the smallest Q to justify a complete interpretation of the Guinier region, but enough to determine its influence on the shape of the observed spectrum. We do not believe that the source of this smallest Q scattering is associated with the oil−surfactant structure which results in the peak and larger Q data. In any case, we intend to extract information on the spatial geometry of the oil−surfactant surface structure from the result of the leveled-wave fit to the peak position and shape.

A Lorentzian function was also used to describe the smallest angle scattering, with the result that although the overall fit was not as adequate as with the Guinier function, the leveled-wave model parameters were only slightly affected. Table 3 gives the results of this fitting. The oil−surfactant compositions do not correspond exactly to the 40/60 oil−surfactant ratio. For this reason, it is not possible to obtain a correlation between the geometry of the oil−surfactant surface and the miscibility gap. However, for the present study, the most significant observation is that the distribution of wave vectors **k** required by the leveled-wave model to describe the oil−surfactant surface structure is significantly different from that produced by the measurement characterizing the aqua−surfactant surface structure.

We conclude that the *oil−surfactant surface and aqua−surfactant surface are of different shapes*, with the oil−surfactant surface having a smaller k_s (i.e., a larger length scale). To the best of our knowledge, this is the first system that clearly shows this behavior. In the only other study[18] in which the two surfaces were studied independently, by the use of alternately deuterated aqua and oil, the peak positions were found to be identical and thus the surfaces to be identical. This effect observed with the system studied here is no doubt due to the size and chemistry of the surfactant.

As with the analysis of the aqua structure resulting from the use of the leveled-wave model, one can produce a spatial geometry of the two components (i.e., with the oil as one and the remainder as the second) and obtain a two-dimensional cut. This is shown in Figure 9 for the data corresponding to oil samples O33 and O12 of Table 3, which are quite representative of all the oil structure data.

The structures resulting from this analysis as depicted in Figures 6 and 9 are rather complicated. We can see that the length scales of the two surfaces are substantially different (different k_s) and that the oil−surfactant surface is rougher (larger Σ) than the aqua−surfactant surface.

Surfactant Structure. Seven samples were prepared in which the triolein oil and the aqua components are deuterated; Table 4 gives their compositions and Figure 10 shows their positions on the Gibbs triangle. Although the neutron contrast

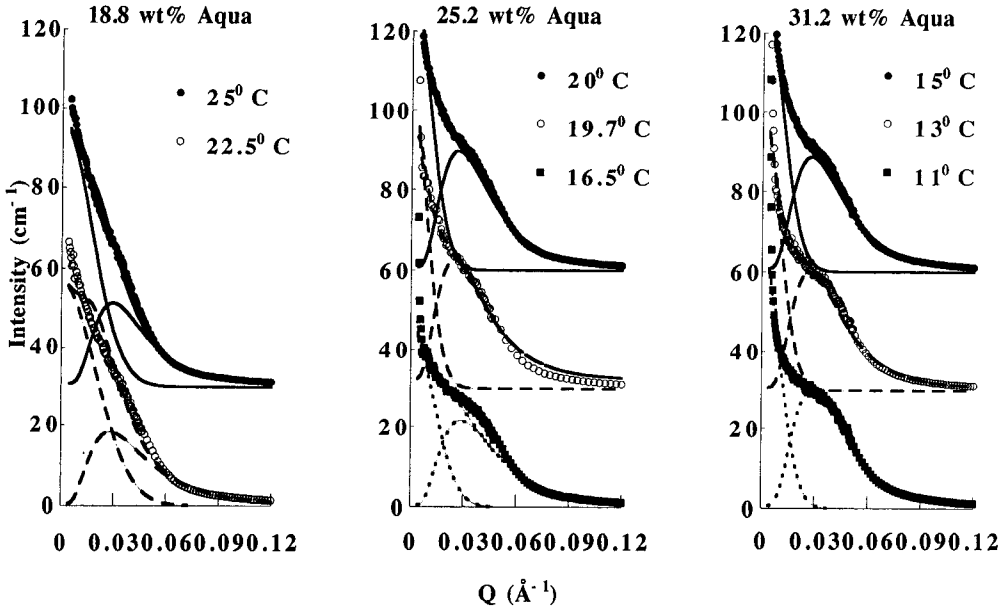

Figure 8. SANS data obtained from three samples used for oil structure determination at several temperatures. Lines are data fit with the leveled-wave model and a Guinier function (see text). There exists a line which is the sum of these two components. If it is not visible, it is due to the fact that it is obscured by the data points. Spectrum for higher temperatures in each figure is displaced vertically by 15 cm^{-1} from the adjacent spectrum.

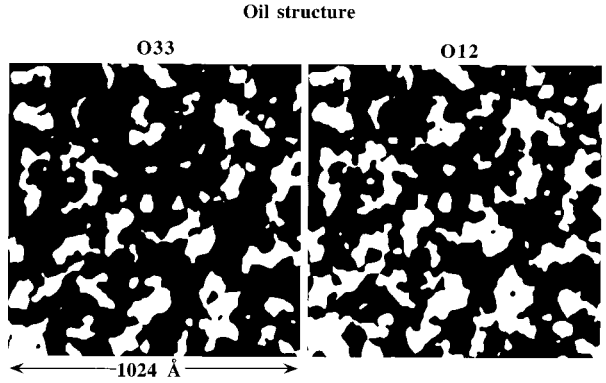

Figure 9. Geometry of the oil component obtained using the log-normal distribution of wave vectors obtained from the leveled-wave model (Table 3). White regions correspond to the aqua component, dark regions to the other two. (See Table 3 for sample labels.)

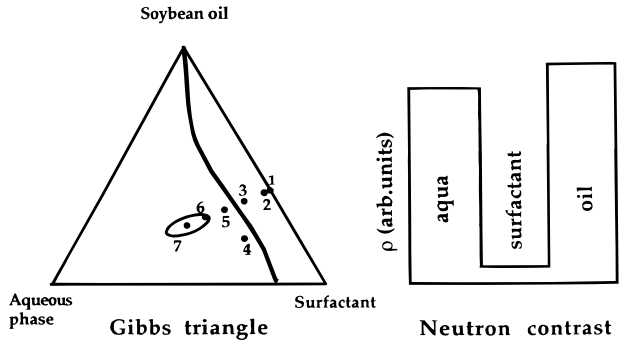

Figure 10. Neutron contrast and composition of seven samples used for measurement of the surfactant structure. Solid lines correspond to 20 °C phase boundaries (Figure 1) (shown for reference).

for the oil and aqua is not quite matched, it is quite different from that of the protonated surfactant; these samples can thus be said to be sensitive to the structure of the surfactant.

We begin with data obtained for the surfactant sample with the lowest aqua concentration, namely, S1, S2, and S3. Data have been obtained for these samples in the temperature range from 5 to 30 °C. As the spectra for these three samples show very little temperature dependence, we present in Figure 11 only

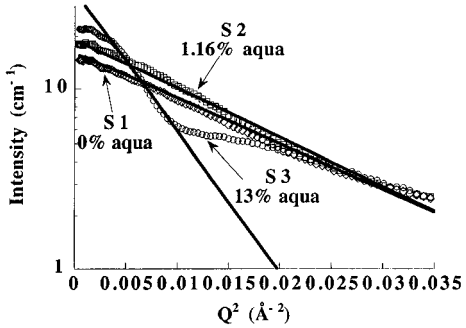

Figure 11. SANS data for three lowest aqua concentrations (samples S1, S2, and S3) of surfactant structure samples (Table 4). The data are plotted on a log scale for $I(Q)$ vs Q^2. Lines are fits with Guinier functions.

the 30 °C data plotted as log(I) versus Q^2. The data are fit in the low-Q region with a Guinier function ($I(Q) = I_{obs} \exp[-(QR_g)^2/3]$), and the fits are shown as the solid lines. The radii of gyration obtained from the fits are $R_g = 13.3$, 13.7, and 23.3 Å, respectively, for the S1 (0% aqua), S2 (1.16% aqua), and S3 (13% aqua) samples. The standard interpretation of scattering that conforms to a Guinier function is that the sample consists of well-dispersed clusters of radius of gyration R_g, which for spheres is related to the radius as $R^2 = (5/3)R_g^2$. This model leads to radii and volumes (R; V) for the three samples of (17.2 Å; 21 300 Å^3), (17.7 Å; 23 230 Å^3), and (30.1 Å; 114 230 Å^3), respectively. If we assume that these structures contain N_a aqua molecules surrounded by N_s surfactant molecules in numbers proportional to their molecular number fraction in the sample, then we obtain (N_a; N_s) of (0; 3.7), (12.8; 3.9), and (648.4; 15.7) for samples S1, S2, and S3, respectively.

These numbers do not seem unreasonable to us. It might have been more reasonable to fit the data for the latter two samples, S2 and S3, with a model consisting of an inner core of aqua surrounded by a shell of surfactant, but the limited data are inadequate for that task. There are, moreover, not enough data to warrant further quantitative interpretation in this Q region. From these data, at the least, one can state that a structure grows larger as the aqua content is increased for small concentrations.

TABLE 4: Surfactant Structure Results and Composition

		log-normal parameters[a]			Guinier parameters[a]		composition[b] (wt %)		
surfactant samples	T (°C)	I (cm^{-1})	Q_s (Å^{-1})	Σ (Å^{-1})	I (cm^{-1})	R_g (Å)	oil, Od	surf, S	aqua, Ad2
S1	30.0				16.0	13.2	40.0	60.0	0.0
S2	30.0				19.0	13.7	39.5	59.3	1.16
S3	30.0				36.0	23.3	34.8	52.2	13.0
S4	20.0	0.271	0.121	0.0423	7.67	32.4	19.3	61.2	19.5
S4	22.5	0.347	0.119	0.0481	7.83	36.2	19.3	61.2	19.5
S4	25.0	0.331	0.118	0.0459	7.09	33.4	19.3	61.2	19.5
S4	27.5	0.356	0.116	0.0484	7.25	35.7	19.3	61.2	19.5
S4	30.0	0.375	0.116	0.0519	7.06	37.1	19.3	61.2	19.5
S5	20.0	0.424	0.110	0.0306	46.2	37.5	31.9	47.8	20.3
S5	22.5	0.524	0.110	0.0360	38.0	33.6	31.9	47.8	20.3
S5	25.0	0.536	0.111	0.0362	34.1	33.1	31.9	47.8	20.3
S5	27.5	0.525	0.111	0.0358	30.6	32.7	31.9	47.8	20.3
S5	30.0	0.445	0.117	0.0316	33.2	32.0	31.9	47.8	20.3
S6	22.5	0.654	0.101	0.0313	32.5	29.8	28.6	42.9	28.5
S6	25.0	0.615	0.102	0.0305	31.0	29.8	28.6	42.9	28.5
S6	27.5	0.880	0.089	0.0368	26.5	28.5	28.6	42.9	28.5
S6	30.0	0.888	0.091	0.0358	28.4	30.9	28.6	42.9	28.5
S7	20.0	2.158	0.054	0.0321	50.0	71.1	25.2	37.8	37.0
S7	24.0	1.834	0.056	0.0363	32.6	42.2	25.2	37.8	37.0
S7	27.5	2.028	0.055	0.0307	35.4	46.7	25.2	37.8	37.0
S7	30.0	1.935	0.051	0.0304	32.7	45.1	25.2	37.8	37.0

[a] See text for models and definition of parameters. [b] See Table 1.

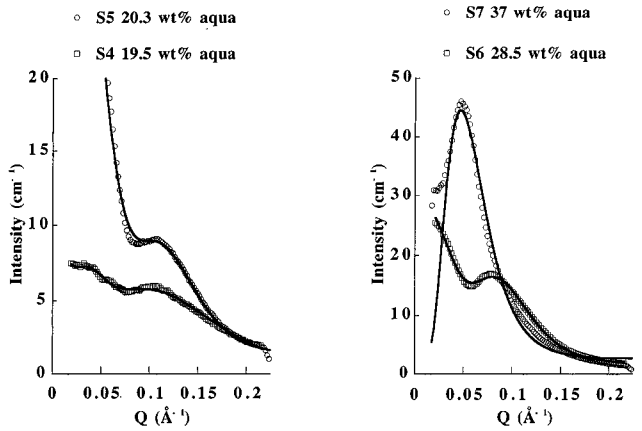

Figure 12. SANS data for four largest aqua concentrations of the surfactant structure samples at 30 °C. Solid lines are fits to data using a Guinier function and a log-normal function of $p(Q)$ (see text); different ordinate scales are used for clarity. See Table 4 for composition and resulting parameters.

In the data for the 13% aqua concentration, it is clear that a second component is developing at a Q greater than ~0.1 Å^{-1}. This develops into a well-defined peak as the aqua concentration is increased for samples S4 through S7, as shown in Figure 12. This figure plots the several spectra obtained at 30 °C. The peak position and width depend on concentration, as they do for the aqua structure sample. It is not possible to analyze these data with the leveled-wave model as presently formulated. As mentioned above, this model assumes that for a three-component microemulsion system (i.e., a system in which the surfaces between the three components also demark surfaces between different neutron contrasts), the two surfaces are described by the same geometry. This is certainly not the case here. There is at present no geometric model formulated that is able to produce a scattering function for a system in which the surfaces bounding the two sides of the surfactant describe different geometries. One might attempt a fit with the Teubner−Strey model.[19] The results of such a fit are similar to those found by Jinnai et al.,[20] namely, that this model does not fit the data. The best we can do at present in order to obtain a "quantitative" comparison between the results of the three contrast samples is to present the position and width of the observed peak.

The determination of the peak position is straightforward for these spectra, since the peak is clearly defined in the data. The width is not as easily determined. All the spectra contain, in addition to the peak, a low-Q component that rises steeply as Q decreases. In choosing a function for fitting the data to obtain peak position and width, we must account for this low-Q component. We have chosen a Guinier function, since it seems to represent the data rather well for all concentrations and temperatures. For the function describing the peak itself, we use the log-normal distribution $I(Q) = I_0 p(Q)$ (of eq 1). We can justify this choice (a) because it seems to work and (b) the spectra $I(Q)$ resulting from the leveled-wave model in the aqua and oil structure samples are well-described by the log-normal distribution. In addition, the data for the lower aqua concentrations contain a weak shoulder at the smallest Q values, which we represent with a second log-normal. The solid lines in Figure 12 are obtained with these functions; Table 4 gives the resulting parameters. We use this procedure to obtain reliable values for the peak position Q_p and standard deviation Σ of the principal peak, which we believe represents the surfactant structure. The fit to the data is quite satisfactory (and well-represented by Figure 12) for all aqua concentrations and temperatures.

One of the most satisfying results of the leveled-wave model was the prediction that the peak in $I(Q)$ would disappear when the oil and aqua volume fractions were equal, these components being formulated with neutron contrast values that are equal, and different from the neutron contrast of the surfactant. The disappearance of this peak had been previously observed but without a satisfactory explanation.[18] This effect exists only if both the surfactant−aqua and surfactant−oil surfaces describe the same geometry. We have presented evidence above that this is not the case here. In the surfactant structure data, we obtain additional evidence that, indeed, these two surfaces are not of the same geometry, in that the peak in $I(Q)$ is ever present as a function of the concentrations of the various components, especially for samples S4 and S6, for which the oil and aqua concentrations are very similar.

Figure 13 presents the values of the peak position Q_p and the standard deviation Σ obtained from the present measurements

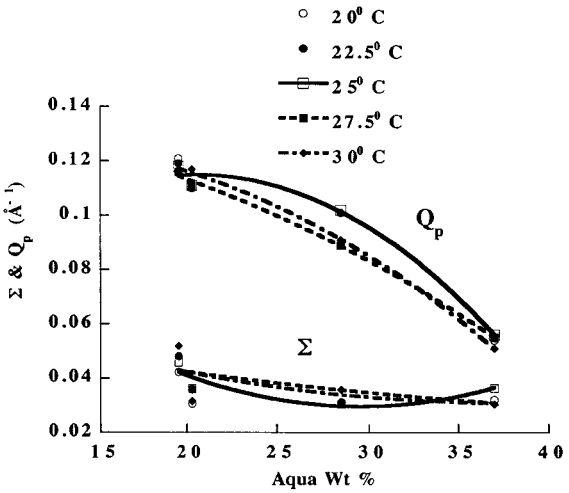

Figure 13. Peak parameters obtained for surfactant structure data plotted as functions of aqua weight fraction for several temperatures. Q_p is the peak position and Σ the standard deviation of the log-normal function used to fit peaks. The lines are guides for the eye obtained with a quadratic function.

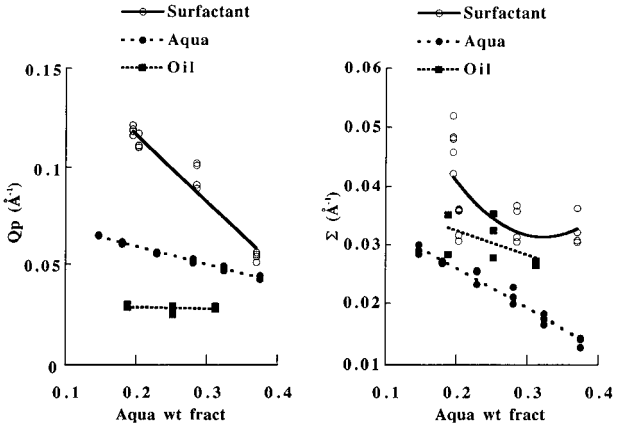

Figure 14. Q_p, the peak position, and Σ, the standard deviation, of the log-normal function $p(Q)$ used to fit $I(Q)$. Data, for all temperatures, are labeled surfactant (Table 4), aqua (Table 2), and oil (Table 3) according to which component they were designed to reveal. (Lines are guides for eye.)

with the surfactant structure samples. This figure can be interpreted as follows. As with the aqua structure geometry, the peak position Q_p exhibits a change in behavior at low temperatures near 25% aqua concentration by weight. This effect is most pronounced at 25 °C. The length scale decreases as the instability in miscibility is approached. The behavior of the standard deviation Σ in this same region of temperature and aqua concentration is, however, different from that of the aqua structure. Here Σ decreases near the instability, again most pronounced at 25 °C. With the interpretation of this parameter as reflecting the width of a distribution of length scales which describe the geometry of the surface, there is an aqua concentration (~25%) for which the surfactant seems to be better ordered. We would like to interpret these observations as a positive correlation between the surfactant structure and the thermodynamic instability in the miscibility; this correlation would provide a mechanism for this phenomenon. To our knowledge, this is the first experimental observation of such a correlation. Without a reliable geometric model, it is difficult to make more definitive statements concerning the behavior of the various surfaces and interfaces. We will only reemphasize that the data themselves indicate that the geometries are correlated with the thermodynamic instability.

Conclusions

We present small-angle neutron scattering data for samples of a microemulsion consisting of triolein oil, aqua (water/ethanol 80/20 wt %) and polyoxyethylene (40) sorbitol hexaoleats. Samples were prepared in which the aqua and oil were deuterated and used to reveal the structure of the aqua, oil, and surfactant structures separately. It was found that the aqua−surfactant and oil−surfactant surfaces do not describe the same geometry at all the compositions used. In addition, a correlation was found between (1) the existence of a thermodynamic instability in the miscibility (phase boundary) and (2) the structural ordering of the aqua−surfactant surface and of the surfactant structure.

To clearly substantiate these claims, we present in Figure 14 the entire set of data (all temperatures) for all three types of samples as a function of aqua weight fraction. In this figure we plot the peak position Q_p and standard deviation Σ that describe the peak in $I(Q)$ resulting from the use of the log-normal function $p(x)$, eq 3. We use these two parameters (rather than those resulting from the leveled-wave model) since they are the only ones available to us for the surfactant structure data. Clearly, the length scales ($2\pi/Q_p$) of the three structures are different, as is the persistence length ($2\pi/\Sigma$).

Acknowledgment. The research at Oak Ridge was supported by the Division of Materials Sciences, U.S. Department of Energy, under Contract No. DE-AC05-840R21400 with Martin Marietta Energy Systems Inc.

References and Notes

(1) Schulman, J. H.; Cockbain, E. G. *Trans. Faraday Soc.* **1940**, *36*, 551.
(2) Friberg, S. E.; Mandell, L. *J. Am. Oil Chem. Soc.* **1970**, *47* (5), 149.
(3) Schwab, A.; Nielson, H. D.; Brooks; Ryde, E. *J. Dispersion Sci. Technol.* **1983**, *4* (1), 1.
(4) Alander, J.; Warenheim, T. *J. Am. Oil Chem. Soc.* **1989**, *66* (11), 1656.
(5) *Ibid.* **1989**, *66* (11), 1661.
(6) Gulik-Krzywicki, T.; Larsson, K. *Chem. Phys. Lipids* **1984**, *35*, 127.
(7) Fontell, K.; Hernqvist, L.; Larsson, K.; Sjoblom, J. *J. Colloid Interface Sci.* **1983**, *93* (2), 453.
(8) Joubran, R.; Cornell, D.; Parris, N. *Colloid Surf., A* **1993**, *80*, 153.
(9) Laughlin Robert G. *The Aqueous Phase Behavior of Surfactants*; Academic Press Inc.: San Diego, 1994. Several examples of this phenomenon are given in Chapter 12.
(10) Trevino, S. F.; Joubran, R.; Parris, N.; Berk, N. F. *Langmuir* **1994**, *10*, (8), 2547, 4398.
(11) Huang, J. S.; Sung, J.; Wu, X. L. *J. Colloid Interface Sci.* **1989**, *132* (1), 34. Kaler, Eric W.; Billman, John F.; Fulton, John L.; Smith, Richard D. *J. Phys. Chem.* **1991**, *95* (1), 458. Baglioni, P.; Gambi, C. M. C.; Goldfarb, D. *Prog. Colloid Polym. Sci.* **1991**, *84*, 133. Baglioni, P.; Dei Luigi; Gambi, C. M. C. *J. Phys. Chem.* **1995**, *99* (14), 5035.
(12) Vaknin, David; Kjaer, KristiAn; Als-Nielsen, Jens; Losche, Mathias *Biophys. J.* **1991**, *59*, 1325.
(13) Chen, S. H. *Annu. Rev. Phys. Chem.* **1986**, *37*, 351.
(14) Koehler, W. C. *Physica (Utrecht)* **1986**, *137B*, 320.
(15) Hammouda, B.; Krueger, S.; Glinka, C. J. *J. Res. N.I.S.T.* **1993**, *98*, 31. A copy of this publication may be obtained from Linda Clutter, Reactor Radiation Div., N.I.S.T., Gaithersuburg, MD 20899.
(16) Johnson, Norman L. *Continuous Univariate Distributions-1*; Houghton Mifflin Co.: Boston, 1970.
(17) Berk, N. F. *Phys. Rev. Lett.* **1987**, *58*, 2718. Berk, N. F. *Phys. Rev. A* **1991**, *44*, 5069.
(18) Auvray, L.; Cotton, J. P.; Ober, R.; Taupin, C. *J. Phys. Chem.* **1984**, *88*, 4586. De Geyer, A.; Tabony, J. *Chem. Phys. Lett.* **1985**, *113*, 83. De Geyer, A.; Tabony, J. *Chem. Phys. Lett.* **1986**, *124*, 357. Auvray, L.; Cotton, J. P.; Ober, R.; Taupin, C. *Physica (Amsterdam)* **1986**, *136B*, 281. Chen, S. H.; Chang, S. L.; Strey, R.; Samseth, J.; Mortensen, K. *J. Phys. Chem.* **1991**, *95* (5), 7427.
(19) Teubner, M.; Strey, R. *J. Chem. Phys.* **1987**, *87*, 3195.
(20) Jinnai, H.; Hashimoto, T.; Lee, D.; Chen S.-H. *Macromolecules* **1997**, *30*, 130.